Journal of
Electronic Imaging

JElectronicImaging.org

Channel-wise barcodes for color display applications

Karthik Dinesh
Jiangfeng Lu
Shingirai Dhoro
Gaurav Sharma

SPIE. IS&T imaging.org

Karthik Dinesh, Jiangfeng Lu, Shingirai Dhoro, Gaurav Sharma, "Channel-wise barcodes for color display applications," *J. Electron. Imaging* **28**(3), 033021 (2019), doi: 10.1117/1.JEI.28.3.033021.

Channel-wise barcodes for color display applications

Karthik Dinesh,[a] Jiangfeng Lu,[a] Shingirai Dhoro,[a] and Gaurav Sharma[a,b,*]
[a]University of Rochester, Department of Electrical and Computer Engineering, Rochester New York, United States
[b]University of Rochester, Department of Computer Science, Rochester, New York, United States

Abstract. We present a channel-wise (CW) framework for data embedding in display images using barcodes. Data are embedded in one or more channels of the color image encoded as a monochrome barcode pattern and extracted from the corresponding channels by the decoder. We highlight two advantageous schemes, realized in the proposed framework: red, green, blue CW barcodes (RGB-CWBs), and blue channel image-barcodes (BC-IBs). Compared with a conventional monochrome black and white barcode BW-B with the same spatial footprint, RGB-CWBs utilize the three channels of color image more effectively and enable a three-fold increase in data rate, whereas BC-IBs significantly reduce the embedding distortion by exploiting the reduced sensitivity of the visual system to spatial detail in blue colors. For RGB-CWBs, we develop an effective framework for the cancellation of cross-channel interference between the display and capture channels using a model for the display and capture processes and for the ambient illumination. Model parameters required for interference cancellation (IC) are learned on-the-fly using either expectation-maximization or through suitable design of the synchronization patterns as "pilot-blocks." Extensive experiments over multiple display and capture devices validate the advantages of the framework: RGB-CWBs (with IC) and the BC-IBs offer bit error rates comparable to their monochrome counterparts while providing either a three-fold increase in data rate or a significant reduction in distortion, respectively. [DOI: 10.1117/1.JEI.28.3.033021]

Keywords: RGB channel-wise barcodes; blue channel image-barcodes; cross-channel interference; S-CIELAB.

Paper 190016 received Jan. 5, 2019; accepted for publication May 10, 2019; published online Jun. 5, 2019.

1 Introduction

The ubiquitous availability of smartphone cameras and widespread prevalence of displays is enabling new display-based applications for barcodes and other machine readable data interfaces.[1] Barcodes encode the data as image patterns offering high data capacity and robust decodability but are visually obtrusive. Image-barcodes[2,3] attempt to reduce the visual obtrusiveness by approximating an image, with a minimal compromise in the robustness of data decodability.

Traditional 2-D barcodes such as the QR code,[4] Aztec code,[5,6] and specially designed 2-D barcodes[7–9] have been used in display applications to enable a variety of functions such as security,[10] visible light communication,[11–13] and automation of point of sale transactions.[14,15] To provide higher data rates, color 2-D barcodes have also been proposed recently for use in both print[16–19] and in displays.[20–22]

The afore-mentioned applications use barcodes without consideration of visual aesthetics. Applications involving marketing and media, where personalization and customer engagement is critical, require visually appealing barcodes. Several barcodes and image-barcodes have been deployed for these applications. Vcode,[23] a video barcode, has been proposed for advertising to increase data capacity and to provide real-time decoding. Picture-embedding barcodes, such as the monochrome PiCode and ViCode[24,25] and ColorCode[26] and Pictorial Image Code[27] color image-barcodes, have been used for display advertising. To make barcodes visually appealing, either the error correction capability of the 2-D barcodes is exploited to replace part of the barcode area with image content,[28] or the intensity of the barcode region is modulated to embed the image content.[29,30] Although these techniques make the barcode visually engaging, for video advertisements, usually the barcode is embedded in a small region of the image and such techniques are not utilized. In the video advertising applications,[31,32] it is desirable to minimize the barcode footprint and/or visual obtrusiveness. Additionally, it is increasingly desirable to embed advertising and product placement within broadcast/streaming content instead of relying on the traditional interruptive advertising model. The introduction of native barcode decoding capability in the camera applications for Android[33] and iOS[34,35] makes display barcodes and image-barcodes attractive for targeted personalized advertising.

In this paper, we propose a channel-wise (CW) barcode framework for embedding information in a displayed color image. For CW barcodes, the data encoded as monochrome barcode pattern are embedded in one or more channels of the image and data are decoded from the corresponding channels using a barcode decoder. We highlight two advantageous realizations of CW barcodes: RGB channel-wise barcodes (RGB-CWBs) and blue channel image-barcodes (BC-IBs). The RGB-CWBs and BC-IBs offer advantages over conventional black and white barcodes BW-Bs, whereas RGB-CWBs offer a three times increase in the data capacity for the same footprint area, BC-IBs exploit the reduced sensitivity of human visual system (HVS) to spatial detail in the blue channel for reducing the perceptual impact. For RGB-CWBs, we develop an effective framework for improving decoding performance by canceling cross-channel interference between the display and capture channels. Based on a physical model for the display and capture processes and for the ambient illumination, we demonstrate that the

*Address all correspondence to Gaurav Sharma, E-mail: gaurav.sharma@rochester.edu

1017-9909/2019/$25.00 © 2019 SPIE and IS&T

effect of cross-channel interference and ambient illumination can be eliminated using an affine color coordinate transform. The parameters for the affine transform are estimated on-the-fly from captured barcode images using either an expectation-maximization (EM) approach or through a suitable design of the synchronization patterns as known colors that serve as "pilot-blocks" for the estimation. The framework we adopt in this paper is inspired by prior work from our group[19] that used the CW framework for printed color barcodes. Use in color displays, however, presents both different challenges and also different opportunities. Specifically, the physics of subtractive color printing based on cyan, magenta, and yellow (CMY) colorants differs from the physics of additive RGB displays, leading to differences in the algorithmic approaches. For printed CMY-CW barcodes, the physical model leads to a linear interference cancellation (IC) transform applied in the optical-density domain, which is obtained via a logarithmic transformation of normalized reflectance estimates obtained from the captured RGB sensor images.[19] For RGB-CWBs, on the other hand, the physical model leads to an affine (linear + offset) IC transform applied directly in the (linear) R, G, B, sensor response space (as developed in Sec. 2). Also the BC-IB is unique to the display setting presented here and enabled by the fact that, for displays, the interference of the R and G channels on the B channel is small. The corresponding Y channel analog is not effective in print: because the Y channel encounters the worse interference, which is often larger than the primary signal.[19] The embedding of the barcodes in images also motivates our consideration and assessment of distortion in this paper, which was not addressed in the prior work on printed barcodes.[19] Compared with our prior work,[19] this paper also presents a complete framework for synchronization and localization for coherent and incoherent embedding options; the latter option being particularly attractive for temporally sequential embedding of barcodes in an uncoordinated fashion (as discussed in Sec. 6) The work presented here also builds upon and advances upon our prior preliminary reports on this research.[36,37] Specifically, the affine model that comprehends ambient illumination is new; two alternative coherent/incoherent constructions are elaborated for RGB-CWBs, and there is extensive consideration of synchronization for the alternative constructions. Additionally, results are reported for a wider set of experiments over a variety of image content and across multiple displays and smartphone cameras.

Although the RGB-CWBs that we present in this paper can be used in a variety of different applications, to unify the discussion with BC-IBs, we present and evaluate both in the context of the target application to video advertising (There is considerable geographic variation in usage of BW-Bs in advertising, whereas usage in US/Europe is currently limited, there is significantly more usage in Asia, particularly China and Japan.[38–40]). Several additional example applications of the RGB-CWBs are highlighted in Sec. 6. To demonstrate the effectiveness of the proposed approach, we perform visual distortion and data recovery assessments and compare against the BW-Bs. QR and Aztec codes, two of the most commonly used barcodes, are utilized in the experiments. Experimental results show that the proposed CW barcodes offer lower visual distortion than BW-Bs (substantially lower for the BC-IBs), whereas they are comparable with regard to data recovery. Although we present the proposed framework in the context of video advertisement application, CW barcodes, especially the RGB-CWBs and other variants of CW barcodes, such as two channel embedded barcodes, can be used in all the applications where traditional 2-D barcodes have been utilized. Another key advantage of the proposed framework is that it can advantageously make use of almost all of the existing functionality designed and optimized for the BW-Bs such as localization, synchronization, and error correction capability.

This paper is organized as follows: details of the data embedding and decoding procedure for the CW barcodes are provided in Sec. 2. The assessment methodology and metrics used to evaluate the proposed CW barcodes framework against BW-Bs are described in Sec. 3. Experimental results are presented in Sec. 4 followed by conclusion in Sec. 5, and discussion in Sec. 6. An appendix, in Sec. 7; includes additional results and supplementary detail.

2 Channel-Wise Barcodes for Display Applications

Although any BW-Bs can be incorporated within the CW barcode design framework, we will use QR codes in our illustrations of the framework and the description of the data embedding and data recovery procedures in the following sections.

2.1 *Data Embedding for CW Barcode*

The data embedding procedure for the proposed CW barcode is shown in Fig. 1. A message m_i is encoded as a BW-B and embedded into an appropriately selected spatial region in one or more channels of a color image to form the proposed CW barcode. CW barcode can be mathematically represented as

$$\tilde{I}_i^d(x,y) = \mathbf{1}_{\mathrm{BC}}(x,y) I_{\mathrm{BC}}^{m_i}(x,y) + [1 - \mathbf{1}_{\mathrm{BC}}(x,y)] I_i^d(x,y). \tag{1}$$

Here, $I_i^d(x,y)$ represents the color image with $i \in \{\mathrm{R,G,B}\}$ representing the channels of the color image. $I_{\mathrm{BC}}^{m_i}(x,y)$ represents the BW-B with encoded message m_i. $\mathbf{1}_{\mathrm{BC}}(x,y)$ represents the indicator function of the spatial region where the barcode $I_{\mathrm{BC}}^{m_i}(x,y)$ is placed. $\mathbf{1}_{\mathrm{BC}}(x,y)$ takes a value of 1 over the subset of pixels BC corresponding to the region where the barcode is inserted and takes a value of 0 for all other pixels. $\tilde{I}_i^d(x,y)$ represents the channel with the embedded barcode. The advantage of the framework is that

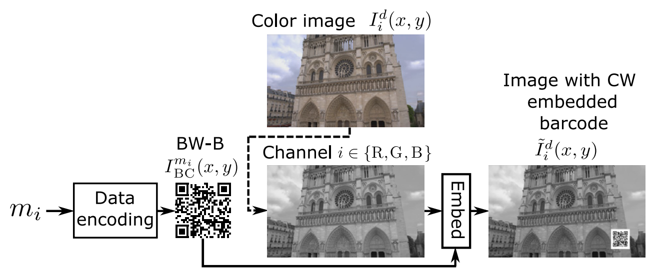

Fig. 1 Data embedding procedure for the proposed CW barcode. A message m_i is encoded into a BW-B $I_{\mathrm{BC}}^{m_i}(x,y)$. The BW-B is embedded in a suitably chosen region $\mathbf{1}_{\mathrm{BC}}(x,y)$ in one or more channels of a color image $I_i^d(x,y)$, $i \in \{\mathrm{R,G,B}\}$ represent red, green, and blue channels, respectively. The resulting CW barcode is represented as $\tilde{I}_i^d(x,y)$, $i \in \{\mathrm{R,G,B}\}$.

we can choose any single or multiple combinations of the channel "i" and message "m_i" to form the proposed CW barcode. One such embedding scenario is to choose $(i, m_i) \in \{(R, m_R), (G, m_G), (B, m_B)\}$, i.e., we choose three BW-Bs $I_{\mathrm{BC}}^{m_R}(x, y)$, $I_{\mathrm{BC}}^{m_G}(x, y)$, and $I_{\mathrm{BC}}^{m_B}(x, y)$ and embed them into R, G, and B channels of the color image, respectively, to form RGB-CWB.[37] Compared with BW-B, the RGB-CWB offers three times the data rate for the same barcode footprint. In another scenario, we retain the image contents in red and green channels and choose $(i, m_i) \in \{(B, m_B)\}$, i.e., a single BW-B $I_{\mathrm{BC}}^{m_B}(x, y)$ is embedded in the blue channel of the color image to form BC-IB.[36] Compared with BW-Bs, the BC-IB offers a lower distortion because of the HVSs reduced sensitivity to spatial detail in the blue channel (As discussed in Ref. 36 depending on image content, other channels could also be advantageously used for CW image-barcodes. Such schemes are straightforward extensions of the approach presented here and therefore not explicitly elaborated upon.).

For the RGB-CWB, we have two variations for the embedding process resulting in two different designs: coherent and incoherent.

2.1.1 *Coherent RGB-CWB*

Figure 2 shows a flow diagram of data embedding process for generating a coherent RGB-CWB. As shown in this figure, the BW-Bs embedded in each of the R, G, and B channels are spatially aligned to the common geometric layout so that the locations of the synchronization pattern in the three channels coincide. Also in the process of embedding the BW-Bs into the R, G, and B channels of the coherent RGB-CWB image, the regions comprising the synchronization patterns are modified. The modifications set the colors of these regions to preselected combinations of R, G, and B and form "pilot blocks (PBs)" of known colors that facilitate decoding by enabling ready estimation of cross-channel color interference parameters. The PB approach was also used for printed CMY-CW barcodes[19] and is inspired by and named after pilot symbols that are used in communication systems for the very similar objective of estimating the channel state.[41] Note that this modification does not impact the data encoded in the barcodes because the synchronization patterns of the BW-Bs do not carry any of the encoded data. Synchronization recovery and interference parameter estimation are addressed later in this section when we consider the decoding process for coherent RGB-CWBs.

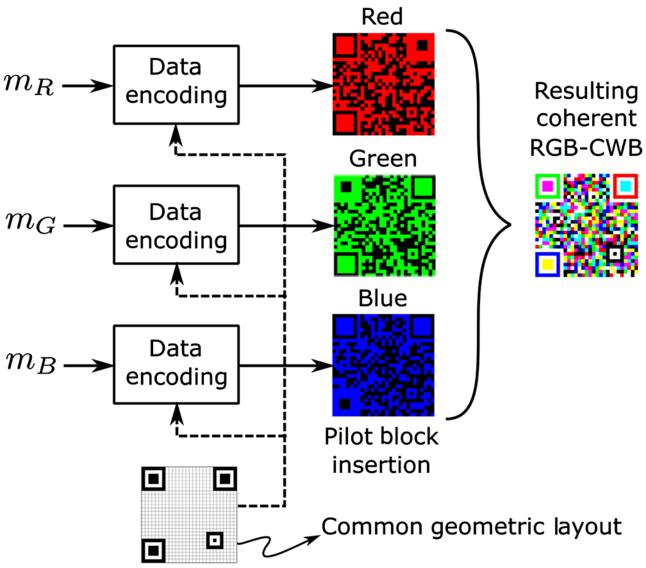

Fig. 2 Data embedding procedure for a coherent RGB-CWB. Messages m_R, m_G, and m_B are encoded as BW-Bs with a common geometric layout. The resulting BW-Bs are embedded in R, G, B channels of the color image. In this process, components of the synchronization pattern are assigned different colors to serve as known "PBs" that can be used to estimate cross-channel interference at the decoder.

2.1.2 *Incoherent RGB-CWB*

The incoherent RGB-CWB construction, shown in Fig. 3, does not need co-ordination of the individual barcodes for the three channels. The incoherent barcode design approach offers greater flexibility because the geometric layout of the synchronization patterns and the data carrying modules in the barcodes for the individual channels can be independent of each other. In fact, the three individual constituent barcodes can also be different types of barcodes, e.g., a QR code in the R channel, an Aztec code in the G channel, and a DataMatrix code in the B channel. Because each of the R, G, B channels carry a complete BW-B, localization of the synchronization patterns in a given channel can be performed individually provided the interference is not excessive. However, because the synchronization patterns are not co-registered, we cannot change the colors for the regions corresponding to the synchronization patterns in order to enable a better estimation of the cross-channel color interference. Hence a more sophisticated method of decoding is required, which is explained later in this section when considering the decoding process for incoherent RGB-CWBs.

2.2 *Data Recovery for CW Barcode*

Once an image of a CW barcode is captured by a camera (usually, smartphone camera) from a displayed image, in which the barcode is embedded, the data are decoded using the procedure outlined in Fig. 4. The first step is

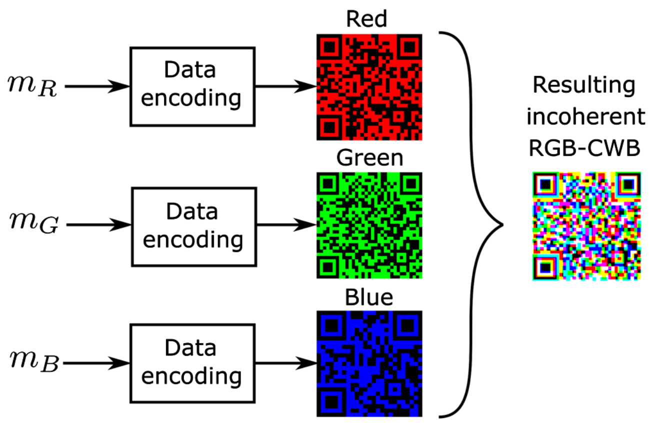

Fig. 3 Data embedding procedure for an incoherent RGB-CWB. Messages m_R, m_G, and m_B are encoded as BW-Bs with individually selected geometric layouts. The barcodes are embedded in R, G, B channels of the color image to form incoherent RGB-CWB.

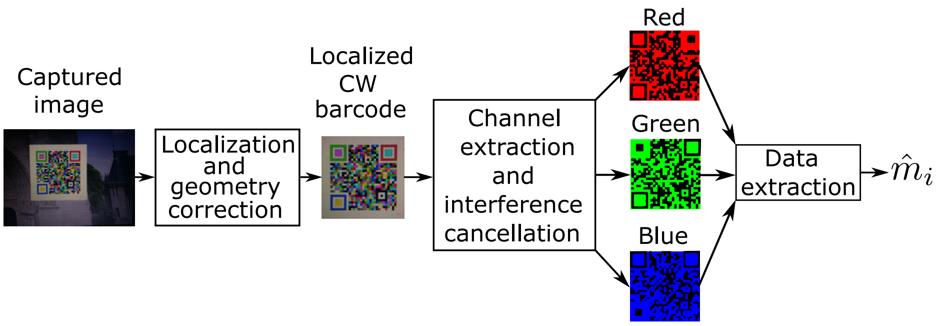

Fig. 4 Data recovery for CW barcodes. The barcode is first localized in the captured image and geometric distortion is corrected. From localized geometry corrected CW barcode, individual channels are extracted and data are recovered, optionally, after IC.

localization and geometric correction, which identifies the spatial region containing the CW barcode and corrects for perspective distortion introduced due to deviations from fronto-parallel geometry for the display and capture camera. The localized CW barcode is separated into R, G, and B channels and data are recovered from the corresponding channels with embedded data.

Ideally, the R, G, B display and capture channels form noninteracting parallel channels, i.e., there are no cross-channel interactions between the display and capture channels. However, in reality, each channel of the captured image has contributions not only from the matching display channel, but also from the nonmatching display channels. We refer to this phenomenon as "cross-channel interference," which sometimes causes a decoding failure when the R, G, B channels of the captured image are directly fed into the decoder software. Apart from cross-channel interference, the captured image also has a contribution from the ambient illumination. The cross-channel interference, particularly, affects the performance of RGB-CWB more than BC-IB. Therefore, for RGB-CWB, we develop a model and methods that allow us to parameterize the interference and cancel it to recover the data.

Before describing the specifics of the modeling, estimation, and correction process, we first describe the overall systems for data decoding for RGB-CWB (coherent and incoherent) and BC-IB.

2.2.1 *Data recovery for coherent RGB-CWB*

Figure 5 shows an outline for data decoding for coherent RGB-CWB. Localization and geometry correction requires estimation of the locations of synchronization patterns in the barcode. As mentioned earlier, for the coherent RGB-CWB, because the synchronization patterns used in the individual channels are manipulated, no single channel contains a complete synchronization pattern. However, the choice of the manipulation can be made such that two properties are met. First, the white regions in the synchronization patterns of the three constituent BW-Bs remain white in the coherent RGB-CWB image. Second, the black regions in the synchronization patterns of the three constituent BW-Bs remain black in at least one of the three R, G, and B channels. When the two properties are satisfied, the image obtained by setting each pixel value to be the minimum of the R, G, and B channel images in the coherent RGB-CWB image preserves the black and white regions of the synchronization patterns. The resulting monochrome image is fed to the decoder to obtain the locations of the synchronization patterns. Utilizing the location parameters, we use standard

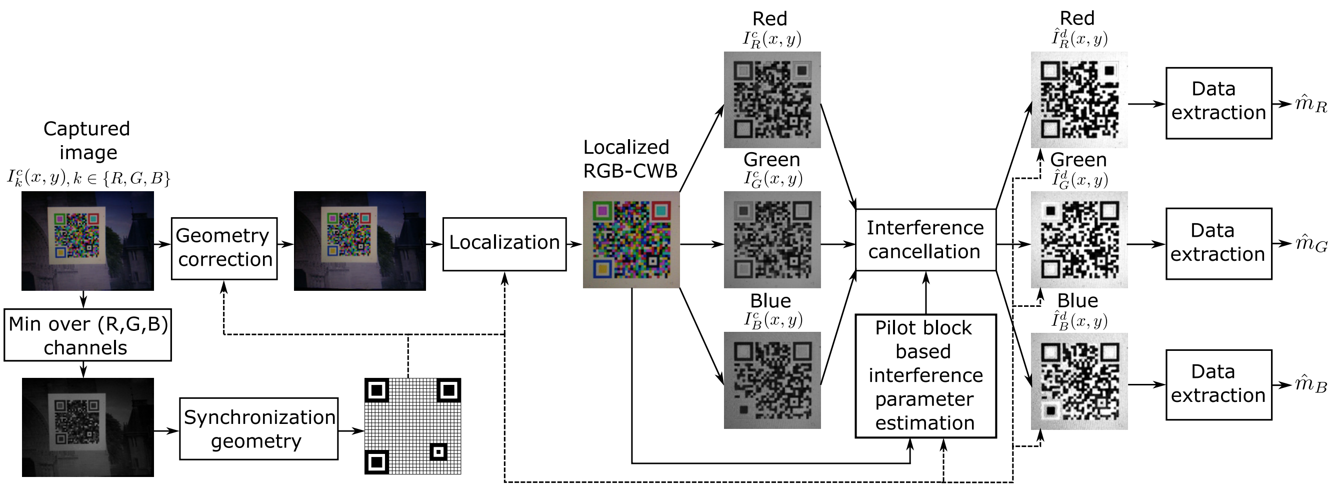

Fig. 5 Data recovery for a coherent RGB-CWB. The region containing the coherent RGB-CWB is first located. After correction of geometric distortion, the PBs are used to estimate the cross-channel interference parameters. Using the parameters, the cross-channel interference is canceled and data are recovered.

algorithms developed for BW-Bs to obtain the transformation matrix, which performs geometry correction to obtain the localized and geometry corrected coherent RGB-CWB.

Once the localized coherent RGB-CWB is obtained, we use the known PB R, G, B values encoded in the synchronization regions in the encoder, to estimate parameters for the cross-channel interference and the contribution of the ambient illumination to the captured image. Details of the estimation procedure are described subsequently in this section. These parameters are utilized to obtain an estimated image, which is free from interference. The interference-canceled image is used along with the geometric layout and alignment information for decoding the data embedded in each channel of the coherent RGB-CWB.

2.2.2 *Data recovery for incoherent RGB-CWB*

Figure 6 shows the procedure of data decoding for incoherent RGB-CWB. Unlike coherent design, the synchronization patterns are fully present in each channel with no modifications. Hence, we can choose either of the three available channels to obtain the location of synchronization patterns. We then perform geometric correction and obtain the localized incoherent RGB-CWB.

We use a subset of pixels from the localized incoherent RGB-CWB and use an EM-type procedure via an alternating least squares process to estimate the cross-channel interference parameters. Similar to coherent design, we also estimate ambient illumination parameters. The procedure to estimate the parameters is discussed subsequently in this section. We next perform IC to obtain an estimate of an interference free incoherent RGB-CWB image. In each channel of the estimated image, the synchronization patterns are intact and hence data can be decoded by the process used for decoding of conventional BW-Bs.

2.2.3 *Data recovery for BC-IB*

For the BC-IB, the BW-B is embedded only in the blue channel. Hence, we utilize the blue channel of the captured image to obtain the location of synchronization patterns. Using the location parameters, we obtain a geometry corrected and localized BC-IB. The localized BC-IB is separated into R, G, B channels and the blue channel is directly fed to the decoder to recover the data.

2.3 *Physical Model for Display-Capture Process*

We rely on a physical model of the display-capture process to develop a parametric representation that enables estimation and cancellation of the effects of the cross-channel interference and ambient illumination. From Eq. (1), we see that the color image created by the CW embedding process has the three channels $\tilde{I}_i^d(x, y)$, $i \in \{\mathrm{R, G, B}\}$. When the image is displayed, the three RGB image channels spatially modulate the corresponding three RGB display channels. Including the effect of ambient illumination (that is reflected off the display), the spatio-spectral distribution of the displayed image can be modeled as

$$\hat{r}(x, y; \lambda) = \sum_{i \in \{\mathrm{R,G,B}\}} \tilde{I}_i^d(x, y) P_i(\lambda) + a_l(\lambda), \tag{2}$$

where $P_i(\lambda)$ is the spectral power distribution for the i'th display channel (primary) and $a_l(\lambda)$ is the spectral power distribution of the ambient illumination. We note that often individual channel image values are nonlinearly encoded through "gamma correction." However, gamma correction has no impact on the barcode regions where the image is a bi-level image taking values 0 or 1.

The image of the displayed CW barcode captured by the camera can be modeled as

$$I_k^c(x, y) = \int s_k(\lambda) \hat{r}(x, y; \lambda) \mathrm{d}\lambda, \tag{3}$$

where $s_k(\lambda)$ represents the spectral sensitivity of the k'th capture channel with $k \in \{\mathrm{R, G, B}\}$. $I_k^c(x, y)$ represents the captured pixel corresponding to k'th camera capture channel. Now by substituting Eqs. (2) into (3), relationship between captured pixel and displayed pixel is represented as

$$I_k^c(x, y) = \sum_{k,i} q_{ki} \tilde{I}_i^d(x, y) + a_k^l, \tag{4}$$

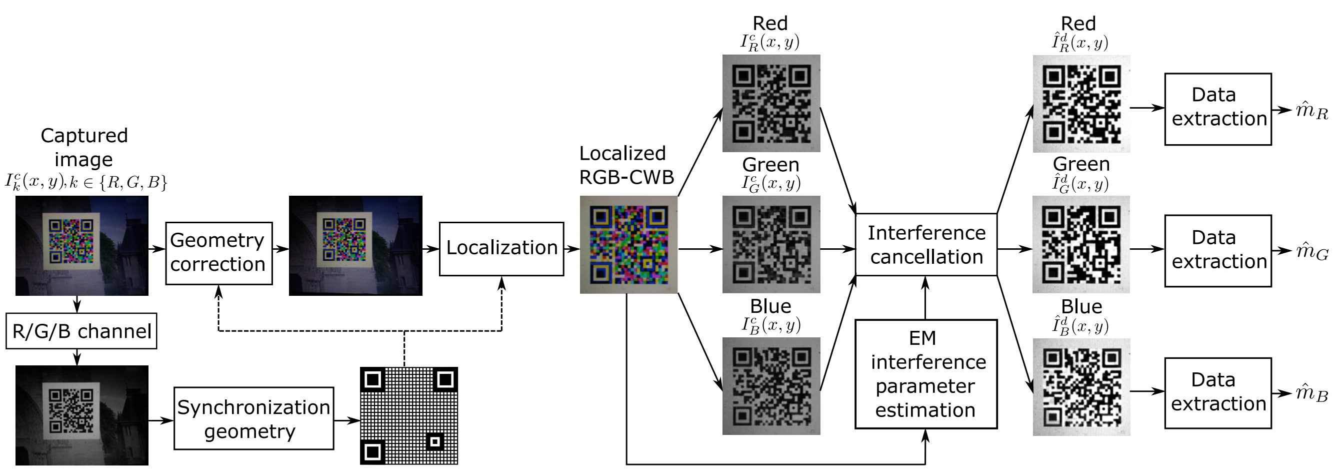

Fig. 6 Data recovery for an incoherent RGB-CWB. The captured image is separated into individual channels where the barcodes are localized and geometric distortion is corrected. Using the EM approach, the cross-channel parameters are estimated. Using the parameters, the cross-channel interference is canceled and data are recovered by decoding the barcode in each channel.

where $q_{ki} = \int s_k(\lambda) P_i(\lambda) \mathrm{d}\lambda$ represents contribution by a display pixel $\tilde{I}_i^d(x, y)$ from i'th display channel to the captured pixel $I_k^c(x, y)$ corresponding to k'th capture channel. The q_{ki} values can be represented as a 3×3 matrix $\mathbf{Q}$, where the i'th column is $[q_{\mathrm{R}i}, q_{\mathrm{G}i}, q_{\mathrm{B}i}]^{\mathrm{T}}$. The matrix $\mathbf{Q} = [q_{ki}]$ models the coupling between the display and capture channels. The diagonal elements in $\mathbf{Q}$ represent the contributions of the display R, G, B channels to the corresponding R, G, B capture channels, and the nondiagonal elements represent the cross-channel interference between display channels and noncorresponding capture channels. The parameter $a_k^l = \int s_k(\lambda) a_l(\lambda) \mathrm{d}\lambda$ for $k \in \{\mathrm{R, G, B}\}$ represents the contribution of ambient illumination to the k'th capture channel. The a_k values can be represented as vector $\mathbf{a} = [a_{\mathrm{R}}^l, a_{\mathrm{G}}^l, a_{\mathrm{B}}^l]$. Given $\mathbf{Q}$ and $\mathbf{a}$, the display channels $\mathbf{v}^d = [I_{\mathrm{R}}^d, I_{\mathrm{G}}^d, I_{\mathrm{B}}^d]$ at a location (x, y) can be obtained from the camera capture channels $\mathbf{v}^c = [I_{\mathrm{R}}^c, I_{\mathrm{G}}^c, I_{\mathrm{B}}^c]$ at that location as the solution $\mathbf{v}_d$ to the system of Eq. (3)

$$\mathbf{Q}\mathbf{v}^d = (\mathbf{v}^c - \mathbf{a}). \tag{5}$$

The model, therefore, characterizes the impact of cross-channel interference and ambient illumination via an affine color-coordinate transform parameterized by the matrix $\mathbf{Q}$ and the vector $\mathbf{a}$. If we set $\mathbf{a} = \mathbf{0}$, the affine model Eq. (5) reduces to the linear model for display capture process used in our prior work.[37]

2.4 *Parameter Estimation*

Based on our model, the process of IC reduces to one of estimating the parameters $\mathbf{Q}$ and the vector $\mathbf{a}$ for use in Eq. (5). Our physical modeling also conveys the insight that the matrix $\mathbf{Q}$ and the vector $\mathbf{a}$ depend on the display and capture devices as well as the ambient illumination. Thus these need to be assessed for the specific imaging setting under which the barcode image is captured. We consider two alternative approaches for estimating these on-the-fly from the captured barcode itself: the PB approach for the coherent RGB-CWB designs and the EM approach for the incoherent RGB-CWB.

2.4.1 *Pilot block approach*

As mentioned in Sec. 2.1.1, for the coherent RGB-CWB the synchronization marker patterns in all the channels are aligned and allocated known colors to form PBs. An example of color allocation for the PBs is shown in Fig. 2, where the colors allocated to the six PBs are three R, G, and B primary colors and combinations RG, RB, and GB of two primary colors. The knowledge of PB color combinations can be leveraged at the decoder to estimate the cross-channel interference matrix $\mathbf{Q}$, which we refer to as the PB approach due to its analogy with pilot symbols used for estimating the state of the channel in communication systems.[41]

We first estimate the parameter $\mathbf{a}$ as a 3×1 vector $\hat{\mathbf{a}}$ of the minimum pixel values in the R, G, and B channels, over the captured coherent RGB-CWB image. To estimate the cross-channel interference matrix $\mathbf{Q}$, we consider pixel locations of the captured RGB-CWB corresponding to the different PBs and represent their known RGB values by a 3×6 matrix $\mathbf{I}^d$ and the corresponding values corresponding to the captured image by a 3×6 matrix $\mathbf{I}^c$. Then based on (5), we expect $\mathbf{Q}\mathbf{I}^d \approx \mathbf{I}^c - \mathbf{a}\mathbf{1}_{6\times 1}^{\mathrm{T}}$, where $\mathbf{1}_{6\times 1}$ denotes a 6×1 vector of 1's. A least squares estimate of $\mathbf{Q}$ can, therefore, be obtained from the PBs (In practice, for $\mathbf{I}^c$ we use averaged values over the six different colored PBs.) as $\hat{\mathbf{Q}} = \arg\min_{\mathbf{Q}} \|\mathbf{Q}\mathbf{I}^d - (\mathbf{I}^c - \hat{\mathbf{a}}\mathbf{1}_{6\times 1}^{\mathrm{T}})\|$.

2.4.2 *EM approach*

For the incoherent RGB-CWB, we formulate the parameter estimation as an EM problem. As in the PB approach, the parameter $\mathbf{a}$ is first estimated as a 3×1 vector $\hat{\mathbf{a}}$ of the minimum pixel values in the R, G, and B channels, over the captured RGB-CWB image. Equation (5) applied to a subset of k pixels from the image, then yields the latent variable model $\mathbf{Q}\mathbf{I}^d = \mathbf{I}^c - \mathbf{a}\mathbf{1}_{6\times 1}^{\mathrm{T}}$, where $\mathbf{I}^c$ represents a $3 \times k$ matrix of RGB values in the captured image for the k pixels and the corresponding $3 \times k$ matrix of RGB values in the displayed image $\mathbf{I}^d$ represents the unobserved latent variables. Using the EM formulation,[42] the matrix $\mathbf{Q}$ can be obtained via the alternating constrained least squares procedure summarized in Algorithm 1, where the relaxed values for $\mathbf{I}^d$ constrained to lie between 0 and 1 can be interpreted as posterior probabilities that the corresponding entries in $\mathbf{I}^d$ are 1. To initialize the estimate of $\mathbf{Q}$, we apply Otsu thresholding[43] to the individual channels in the captured barcode image to get a crude estimate of the corresponding displayed RGB image and use the least square procedure described for the PB approach over the k pixels to obtain the initial estimate $\mathbf{Q}^1$. The EM algorithm iterates until

Algorithm 1 EM-type algorithm to estimate **Q** and **a**

Input: $3 \times k$ matrix $\mathbf{I}^c$ of RGB values from k pixels in the captured RGB-CWB

Output: $\hat{\mathbf{Q}}$,$\hat{\mathbf{a}}$

begin

$\hat{a}_k \leftarrow \min_{x,y} I_k^c(x, y), k \in \{\mathrm{R, G, B}\}$;

$\hat{\mathbf{a}} \leftarrow [a_{\mathrm{R}}, a_{\mathrm{G}}, a_{\mathrm{B}}]$;

Initialize $\mathbf{Q}^1$.

$n \leftarrow 1$;

repeat

$\mathbf{I}^{d,n} \leftarrow \arg\min_{\mathbf{I}^d} \|\mathbf{Q}^n\mathbf{I}^d - (\mathbf{I}^c - \hat{\mathbf{a}}\mathbf{1}^{\mathrm{T}})\|^2$

subject to $0 \leq \mathbf{I}^d \leq 1$

$\mathbf{Q}^{n+1} \leftarrow \arg\min_{\mathbf{Q}} \|\mathbf{Q}\mathbf{I}^{d,n} - (\mathbf{I}^c - \hat{\mathbf{a}}\mathbf{1}^{\mathrm{T}})\|^2$

subject to $0 \leq \mathbf{Q}$

$n \leftarrow n + 1$;

until $\|\mathbf{Q}^{n+1}\mathbf{I}^{d,n} - (\mathbf{I}^c - \hat{\mathbf{a}}\mathbf{1}^{\mathrm{T}})\|^2 < \tau$;

$\hat{\mathbf{Q}} \leftarrow \mathbf{Q}^n$

end

the model residual $\|\mathbf{Q}\mathbf{I}^d - (\mathbf{I}^c - \hat{\mathbf{a}}\mathbf{1}_{6\times 1}^{\mathrm{T}})\|^2$ falls below a predetermined convergence threshold τ.

2.5 *Interference Cancellation and Decoding*

Using the estimate of the cross-channel interference matrix $\hat{\mathbf{Q}}$, Eq. (5) can be solved for every captured pixel of the coherent and incoherent RGB-CWB to the estimate of the corresponding displayed pixel R, G, B values, free from interference. After IC, we obtain three monochrome images, which correspond to the estimates $\hat{I}_{\mathrm{R}}^d(x,y)$, $\hat{I}_{\mathrm{G}}^d(x,y)$, and $\hat{I}_{\mathrm{B}}^d(x,y)$ of the encoded barcode patterns in the individual channels. The barcode data in these individual channel images can be independently decoded in conjunction with the already obtained synchronization information.

3 Assessment Methodology and Metrics

Motivated by our primary target application of video advertising, we assess the proposed CW barcodes with regard to both their visual distortion assessment and data recovery performance. Also motivated by the application setting, as test images for embedding, we utilize a set of 18 keyframes extracted from the ultra high-definition HEVC DASH data set[44] with 1080 p (1080×1920) resolution and consider two operation modes. We refer the first mode as "active viewer" mode where the viewer captures the CW barcode from close to the screen ($\sim$18 in.). For the "active viewer" mode, we make the barcode smaller ($\approx$30 mm on each side) and place it near the bottom right corner, which is typical of current television advertisements that use BW-Bs. The second mode is referred to as the "couch potato" mode where the viewer captures the displayed CW barcode from a typical viewing distance, which we choose to be 1.5 times the screen diagonal size. Since we capture the CW barcode from relatively large viewing distance in this mode, we make the barcode larger ($\approx$50 mm on each side) and allow it to be flexibly placed anywhere on the screen. The 50-mm barcode, used for the couch potato mode, occupied $\sim$1.9% of the display area and was placed in the low-saliency region of the image. The 30-mm barcode, used for active viewer mode, occupied $\sim$0.5% of the display area. For both modes, we include a uniform border around the CW barcodes to facilitate synchronization, which results in a 15% increase in each dimension. Figure 7 shows the barcode size and placement for couch potato and active viewer modes. Figure 8 shows an example image where either (a) an RGB-CWB, or (b) a active viewer BC-IB, or (c) a couch potato BC-IB, or (d) a baseline (active viewer) BW-B has been embedded. From a comparison of these images, it can be readily appreciated that the active viewer BC-IB offers a significantly lower visual distortion compared to the baseline active viewer BW-B with the same data rate. The couch potato BC-IB also offers a relatively low-visual distortion by exploiting the less salient regions for embedding. Finally, the RGB-CWB maintains the same spatial footprint as the active viewer BW-B but carries three times the data.

URL's are chosen as messages that are encoded into the BW-Bs. The evaluations were performed with QR and Aztec codes because of their widespread use in mobile applications; results for the QR codes are presented here and those for the Aztec code are in Sec. 7. These barcodes make use Reed–Solomon error correction codes[45] and experiments included two error correction levels that correct upto 7% and 25% errors, approximately. RGB-CWBs were generated using barcodes with both sizes and error correction levels, whereas BC-IBs were generated using a barcode with both sizes at a 25% error correction level.

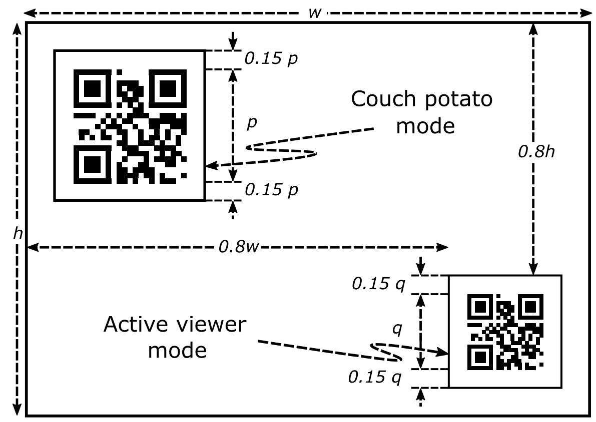

Fig. 7 Barcode placement and size for the two usage modes investigated in our experiments. The couch potato mode (top left) uses a larger size barcode that occupies 1.9% of the display area ($p = \sqrt{0.019wh}$) and is placed in a less salient region of the displayed image. The active viewer mode barcode uses a smaller barcode that occupies 0.5% of the display area ($q = \sqrt{0.005wh}$) and is located near the right bottom corner as shown. In both modes, a 15% surrounding border is added to the barcodes as illustrated. The combination of the barcode and the border defines the region BC of pixels over which the indicator function $I_{\mathrm{BC}}^{m_i}(x,y)$ in Eq. (1) takes a value of 1.

We assess both the visual distortion and data recovery performance for the CW barcodes and compare against corresponding metrics computed for a baseline method that uses a BW-B with sizes, placements, and capture distances identical to that of the CW barcodes.

3.1 *Visual Distortion Assessment*

Visual distortion is quantified using S-CIELAB[46] combined with the CIEDE2000 color difference metric.[47,48] S-CIELAB is a spatial extension of the perceptually uniform CIELAB[49] color space, which models the spatio-chromatic sensitivity of the HVS. To obtain an S-CIELAB representation of a color image, first, color transformation is applied to the image to obtain three opponent channel images (one luminance and two chrominance components). Each of the opponent channel images is passed through spatial filters with their characteristics selected based on the spatio-chromatic sensitivity of the HVS to each of the opponent channel images. Finally, we obtain the S-CIELAB representation of a color image by transforming the filtered images into CIELAB on a pixel-by-pixel basis. To obtain spatio-chromatic differences between two images, we compute the difference between their S-CIELAB representations. To quantify the magnitude of perceived differences between an original image and a CW barcode, we compute the CIEDE2000 color differences between the S-CIELAB representations pixel-by-pixel, to obtain a ΔE error image. The CIEDE2000 provides better perceptual uniformity and, for our setting, also mitigates specific known problems in CIELAB where Euclidean distances in the dark blue regions have a poor correlation with perceived color differences.[50] From the ΔE error image, we

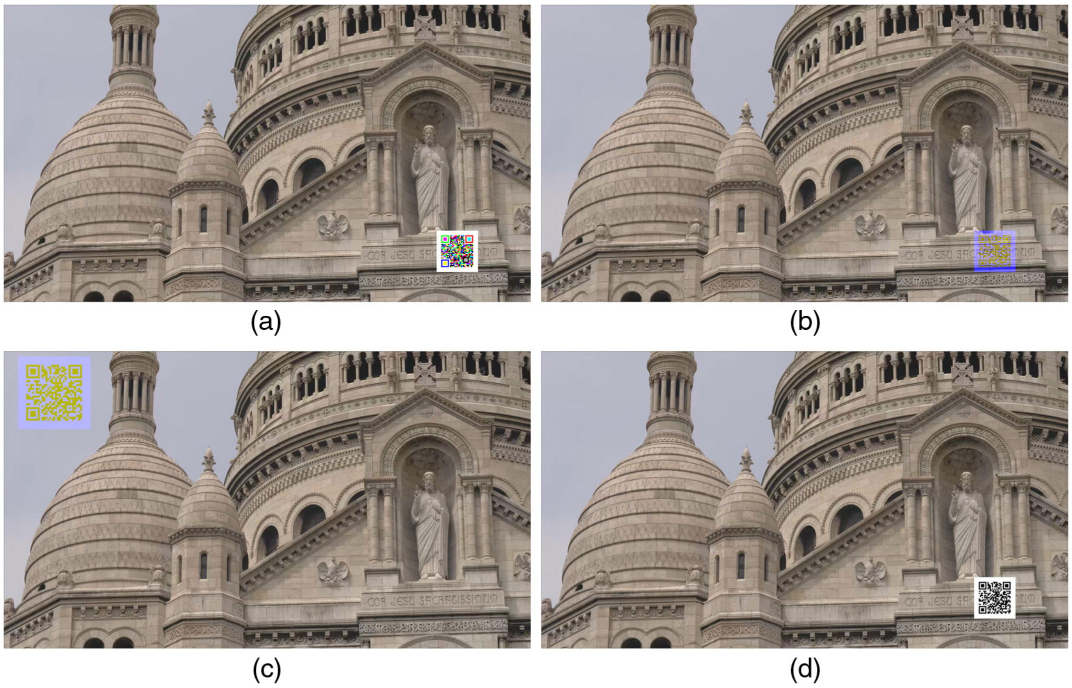

Fig. 8 Image with (a) an RGB-CWB, or (b) an active viewer BC-IB, or (c) a couch potato BC-IB, or (d) a baseline (active-viewer) BW-B embedded.

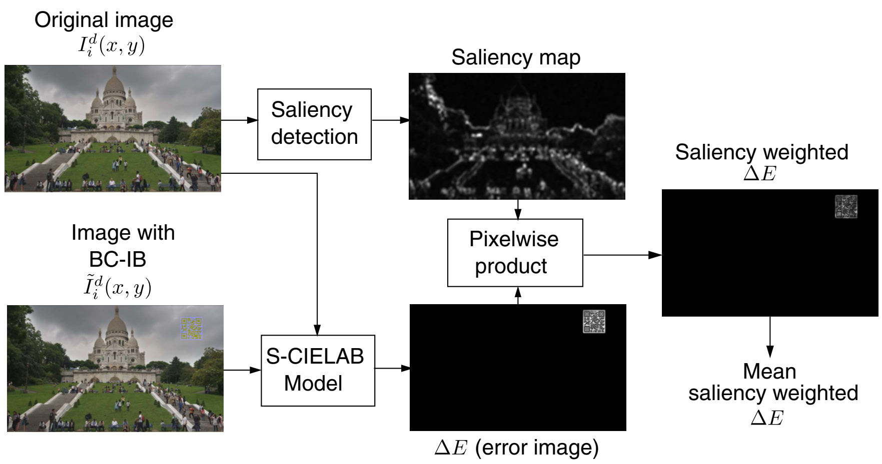

Fig. 9 Saliency weighted S-CIELAB-CIEDE2000 error between original image and BC-IB. The same metric is used to quantify the visual distortion for the RGB-CWBs and baseline BW-Bs.

compute a direct arithmetic average and a saliency weighted average that weights the ΔE error image by saliency at each pixel. Figure 9 shows the overall procedure of visual distortion assessment using BC-IBs for illustration; the same procedure is followed for RGB-CWBs and baseline BW-Bs.

3.2 *Data Recovery Assessment*

To numerically quantify data recovery performance, we utilize synchronization success rate (SSR), bit error rate (BER), and decoding success rate (DSR) as evaluation metrics, which are defined as follows. The SSR is the percentage of captured barcodes in which the decoder is able to synchronize successfully, i.e., correctly localize the barcode based on the patterns that mark its position. The BER is the percentage of bits in error in the bit streams recovered from synchronized barcodes. The BER is computed by comparing the recovered bit stream against the original bit stream embedded in the barcode before any error correction decoding. The third metric, DSR, is the percentage of captured and synchronized barcodes that decode successfully after error correction.

4 Experimental Results

The experiments were conducted on nine different displays of various size and resolution and four different smartphones with specifications as listed in Table 1. As indicated previously, the distance of capture is ~18 in. for the active viewer mode and 1.5 times the display diagonal size for couch

Table 1 List of displays and smartphones used in the experiments.

Displays	Resolution (pixels)	Size (in.)	Smartphones	Resolution (MP)
Dell inspiron (L1)	1080×1920	15	Motorola (M1)	8
Microsoft surface I (L2)	3000×2000	13.5	Samsung (S1)	12
MacBook pro 2017 (L3)	1600×2560	13.3	Iphone X (A1)	12
Asus desktop (D1)	1080×1920	24	Iphone 5s (A2)	8
Dell desktop (D2)	1024×1280	18		
Sun microsystems CRT (C1)	1024×1280	20		
Apple Ipad fifth gen. (T1)	1536×2048	9.7		
Sharp TV (V1)	1080×1920	60		
NEC projector (P1)	1200×1920	106		

potato mode. For the television (T1) and projector (P1), we capture only in couch potato mode.

4.1 *Visual Distortion*

For each display, visual distortion was computed in (SCIELAB-CIEDE2000) ΔE units as described in Sec. 3 using a viewing distance of 1.5 times the screen diagonal size. The saliency weighted averages used the weighting map obtained from the original image using the quaternion DCT-based method.[51]

A total of 144 QR code embedded CW barcodes were used in visual distortion experiments. The 144 images comprise 36 images each of coherent RGB-CWBs, incoherent RGB-CWBs, BC-IBs, and baseline BW-Bs. Table 2 shows the visual distortion result for the QR code embedded CW barcodes for different modes, display sizes, and viewing distances. This table compares the average ΔE and saliency weighted average ΔE for CW barcodes and baseline BW-Bs.

Compared with the baseline BW-Bs, the BC-IBs have a significantly lower visual distortion. For the couch potato mode, the average ΔE is 1.07 and 2.05 for BC-IBs and baseline BW-Bs, respectively—almost 50% lower for the BC-IBs. For the active viewer mode, the average ΔE is 0.50 and 0.78, respectively, for BC-IBs and baseline BW-Bs. Placing the barcode in the salient region proves to be advantageous as the saliency weighted mean ΔE for the couch potato mode becomes less than the mean ΔE and saliency weighted mean ΔE for the active viewer mode. For the couch potato mode, the saliency weighted ΔE is 0.34 and 0.64 for the BC-IBs and the baseline BW-Bs, respectively. For the active viewer mode, the saliency weighted average ΔE is 0.45 and 0.71 for the BC-IBs and the baseline BW-Bs, respectively. The afore-mentioned results demonstrate the advantage of using the BC-IBs in applications where it is desirable to minimize perceptual obtrusiveness.

We also estimate the mean ΔE and saliency weighted mean ΔE for the coherent and incoherent designs of the RGB-CWBs. From Table 2, we can observe that the visual distortion for both coherent and incoherent RGB-CWBs is marginally higher than that of the baseline BW-Bs. Placing the RGB-CWBs in the salient region reduces the distortion for both modes, however, the values for the RGB-CWBs stay marginally worse than that of the BW-Bs.

4.2 *Data Recovery*

4.2.1 *RGB-CWBs*

For RGB-CWB data recovery experiments, from the set of 18 keyframes, we choose four keyframes, in which the barcodes are embedded to form RGB-CWBs (both coherent and incoherent). The four keyframes are chosen in such a way that two keyframes have a dark background, whereas the remaining have lighter background. We choose keyframes with different backgrounds to highlight the dependency of the cross-channel interference on the background level. All combinations of displays, smartphones, barcode modes, error correction levels, and designs result in a total of 1120 images of RGB-CWBs (560 coherent and 560 incoherent RGB-CWBs). In addition, a total of 1536 baseline BW-Bs were captured. We captured two separate sets of QR RGB-CWBs and baseline BW-Bs resulting in an experiment performed on 2240 (1120×2) RGB-CWBs and 3072 (1536×2) BW-Bs.

We evaluate the data recovery performance of the RGB-CWBs using the metrics described in Sec. 3. The data recovery performance of RGB-CWBs is evaluated and compared with baseline BW-Bs for various decoding options. Specifically, RGB-CWBs were decoded either without IC or with IC with the PB approach for coherent RGB-CWBs and the EM approach for incoherent RGB-CWBs. IC considered, alternatively, both the linear and affine models described in Sec. 2. In our experiments, we observed that, consistent with the physical modeling description in Sec. 2, we observed a gain for the affine model when the level of ambient illumination was high. These situations were infrequent in our tests, and hence the difference between these two modes is quite small in the average results summarized

Table 2 Mean and saliency-weighted-mean S-CIELAB-CIEDE2000 ΔE estimates for the proposed QR code embedded CW barcodes and baseline QR BW-Bs for different modes, display configurations, and typical viewing distance, which is ~1.5 times the screen diagonal size. Note that different configurations that coincide with regard to the angular visual field subtended on the eye have the same distortion metrics.

			Mean ΔE				Salience weighted mean ΔE			
Barcode mode	Display size/ resolution (in./ppi)	Viewing distance (in.)	BC-IB	Coherent RGB-CWB	Incoherent RGB-CWB	Baseline BW-B	BC-IB	Coherent RGB-CWB	Incoherent RGB-CWB	Baseline BW-B
Couch potato	15/105 (L1)	21	1.03	2.13	2.10	2.04	0.33	0.67	0.66	0.64
	13.5/227 (L2)	19	1.11	2.19	2.15	2.08	0.36	0.70	0.68	0.66
	13.3/267 (L3)	19	1.14	2.22	2.17	2.09	0.38	0.71	0.69	0.66
	9.7/264 (T1)	15	1.10	2.18	2.14	2.07	0.35	0.69	0.68	0.65
	20/82 (C1), 18/91 (D2)	30,27	1.04	2.13	2.11	2.04	0.33	0.67	0.66	0.64
	106/21 (P1), 60/37 (V1), 24/92 (D1)	159, 90, 36	1.07	2.15	2.12	2.05	0.34	0.68	0.67	0.64
Active viewer	15/105 (L1)	21	0.46	0.79	0.80	0.75	0.42	0.72	0.73	0.69
	13.5/227 (L2)	19	0.54	0.86	0.87	0.82	0.49	0.78	0.79	0.75
	13.3/267 (L3)	19	0.57	0.88	0.89	0.84	0.52	0.81	0.81	0.77
	9.7/264 (T1)	15	0.53	0.85	0.85	0.81	0.48	0.77	0.78	0.74
	20/82 (C1), 18/91 (D2)	30, 27	0.47	0.80	0.81	0.76	0.43	0.73	0.74	0.69
	106/21 (P1), 60/37 (V1), 24/92 (D1)	159, 90, 36	0.50	0.82	0.83	0.78	0.45	0.75	0.75	0.71

here. In the remainder of this discussion, we, therefore, use IC to refer to the affine IC mode.

Table 3 shows the average percentage BER, BER*, SSR, and DSR for red, green, and blue channel estimates of QR coherent RGB-CWBs, and baseline BW-Bs for different modes and error correction levels. BER* denotes the BER computed over RGB-CWBs, in which successful synchronization is accomplished both when using IC or without IC; this provides a comparison of BER on the same set of barcodes with IC and without IC, allowing for a more direct assessment of the benefit of IC. Overall, similar trends are observed for BER and BER*; the following discussion, therefore, refers only to BER. The "PB linear" and "PB affine" columns in this table represent the metrics estimated when linear and affine models are used and data are decoded using the pilot block interference cancellation (PB-IC) technique. The "No IC" column represents metrics for data decoding without using any IC technique.

We first note that the observed BERs for the proposed coherent RGB-CWB are quite small, both with and without IC, and, typically, these BERs are well within the error correcting capability of the error correction codes used in the barcodes. The average BER for coherent RGB-CWBs decoded using PB-IC is significantly lower than BER when decoded without IC. When PB-IC is used, the maximum average BER is 0.97% compared with 3.14% when decoded without IC. The maximum average BER for the baseline BW-Bs is 1.21%. Thus we see that with PB-IC coherent RGB-CWBs have a BER comparable to (actually slightly better than) the BER for the baseline BW-Bs. Comparing the BER performance across individual channels, we observe that the BER is larger for the red and blue channels compared with the green channel, irrespective of barcode modes and error correction levels.

The SSR for coherent RGB-CWBs decoded using PB-IC improves in comparison with SSR when decoded without IC. However, the SSR for coherent RGB-CWBs is slightly worse when compared with SSR for baseline BW-Bs. We also observe a similar SSR trend for the individual channel estimates. The average DSR for coherent RGB-CWBs, when decoded using PB-IC, is higher than DSR when decoded without IC. The minimum average DSR, when decoded using PB-IC, is 92.8%, which is a significant improvement in comparison with DSR of 78.5% when decoded without IC. However, the baseline BW-Bs have a higher average DSR, with a minimum value of 98.4% over the different barcode configurations. The DSR for individual channel

Table 3 Average percent BER, SSR, and DSR for QR coherent RGB-CWBs decoded using PB IC and without any IC. The results are presented for the linear and affine models for IC, different barcode modes, different error correction levels, and for different display-smartphone combinations. The corresponding data recovery metrics for the baseline QR BW-Bs are also indicated.

			Estimated red			Estimated green			Estimated blue			
			IC			IC			IC			
Barcode mode	Error corr. level	Metrics (%)	PB linear	PB affine	No IC	PB linear	PB affine	No IC	PB linear	PB affine	No IC	Baseline
Couch potato	L	BER	0.34	0.34	0.30	0.05	0.04	0.25	0.53	0.52	0.85	0.71
		BER*	0.09	0.08	0.30	0.05	0.04	0.25	0.53	0.53	0.85	—
		SSR	97.4	97.4	95.2	98.3	98.3	98.3	98.3	98.7	96.9	99.9
		DSR	98.7	98.7	87.1	100	100	93.3	99.1	98.7	86.0	99.7
	Q	BER	0.17	0.17	1.05	0.07	0.06	0.47	0.92	0.91	1.38	1.21
		BER*	0.17	0.17	1.05	0.07	0.06	0.48	0.93	0.92	1.36	—
		SSR	98.2	98.2	97.3	97.3	96.9	98.2	96.9	97.3	97.3	100
		DSR	99.5	99.5	91.7	99.5	99.5	98.2	98.1	98.2	87.6	99.5
Active viewer	L	BER	0.22	0.22	0.51	0.10	0.09	0.25	0.62	0.62	0.71	0.81
		BER*	0.21	0.21	0.51	0.09	0.08	0.25	0.64	0.64	0.73	—
		SSR	97.8	98.2	96.7	98.2	98.2	97.1	92.3	92.6	93.7	99.7
		DSR	97.4	97.4	87.0	98.5	98.5	93.5	96.8	95.6	86.2	98.4
	Q	BER	0.97	0.96	2.39	0.45	0.43	0.46	0.96	0.97	3.14	1.20
		BER*	0.76	0.74	2.38	0.25	0.22	0.46	0.93	0.94	3.15	—
		SSR	94.8	94.8	94.7	94.4	95.1	94.4	94.4	94.0	94.0	99.7
		DSR	93.7	93.7	89.3	98.0	97.6	97.2	92.9	92.8	78.5	98.5

estimates is also better for decoding with IC when compared with decoding without IC. The green channel has the best DSR in comparison with red and blue channels.

Table 4 shows the average BER, BER*, SSR, and DSR for red, green, and blue channel estimates of QR incoherent RGB-CWBs and baseline BW-Bs for different modes and error correction levels. The EM linear and EM affine columns represent the metrics estimated when linear and affine models are used and data are decoded using the expectation-maximization-interference-cancellation (EM-IC) technique. Just as was observed in the case of coherent barcodes, the observed BERs for the proposed incoherent RGB-CWB are quite small, both with and without IC, and, typically, these BERs are well within the error correcting capability of the error correction codes used in the barcodes. Also similar to coherent RGB-CWBs, incoherent RGB-CWBs decoded using EM-IC have a lower overall and maximum average BER than those decoded without IC. Also when EM-IC is used, incoherent RGB-CWBs have a slightly lower BER when compared with BER for baseline BW-Bs. For individual channel estimates, we can observe that the BER for green channel is slightly higher when compared with BER for other channel estimates. One of the reasons for higher BER for green channel is due to the design of incoherent RGB-CWBs, where the green channel barcode had the smallest module size (because it had the longest URL).

The overall average SSR/DSR performance for the incoherent RGB-CWBs follow a trend similar to that of coherent RGB-CWBs. The SSR/DSR for incoherent RGB-CWBs, when decoded via EM-IC, is higher when compared with SSR/DSR when decoded without IC and slightly worse when compared with the SSR/DSR for baseline BW-Bs.

In Tables 3 and 4, the BER is slightly lower for the RGB-CWBs compared with the BW-Bs, which is unexpected. The anomaly can, however, be understood by also examining the SSR and noting that the BER can only be computed once synchronization has been achieved (as mentioned in Sec. 3.2). The BW-Bs have a higher SSR compared to RGB-CWBs. The BW-Bs achieve synchronization more often but encounter a higher error rate once synchronized, whereas the RGB-CWBs synchronize less frequently but encounter a lower error rate once synchronized. From an

Table 4 Performance of the proposed QR incoherent RGB-CWBs decoded using EM IC and without any IC, and comparison against the baseline BW-Bs. For a description of the reported metrics and schemes, see the caption for Table 3.

			Estimated red			Estimated green			Estimated Blue			
			IC			IC			IC			
Barcode mode	Error corr. level	Metrics (%)	EM linear	EM affine	No IC	EM linear	EM affine	No IC	EM linear	EM affine	No IC	Baseline
Couch potato	L	BER	0.30	0.23	0.99	0.37	0.40	0.94	0.38	0.61	2.59	0.71
		BER*	0.34	0.26	0.99	0.38	0.41	0.75	0.40	0.69	2.64	-
		SSR	93.6	94.9	81.6	88.0	88.0	94.4	91.0	93.6	82.1	99.9
		DSR	97.7	96.9	92.7	90.8	88.4	95.9	98.1	97.7	95.3	99.7
	Q	BER	0.73	0.69	1.64	0.55	0.47	0.77	0.21	0.21	0.65	1.21
		BER*	0.69	0.64	1.61	0.55	0.47	0.78	0.14	0.14	0.65	-
		SSR	90.8	91.2	71.6	98.7	98.7	98.7	95.8	95.0	80.3	100
		DSR	98.2	99.1	95.9	99.2	100	99.2	99.6	99.6	96.4	99.5
Active viewer	L	BER	0.30	0.34	0.55	0.53	0.63	0.97	0.20	0.20	0.24	0.81
		BER*	0.28	0.28	0.51	0.57	0.68	1.09	0.19	0.18	0.24	-
		SSR	93.3	94.4	91.1	84.1	85.9	88.2	94.8	96.7	93.7	99.7
		DSR	96.8	96.5	94.7	86.3	85.8	86.6	100	99.6	97.6	98.4
	Q	BER	0.74	0.47	0.72	0.97	1.02	1.29	0.15	0.18	0.40	1.20
		BER*	0.33	0.35	0.62	0.96	1.01	1.30	0.13	0.16	0.39	-
		SSR	92.3	91.6	86.2	99.6	99.2	98.5	97.7	97.7	95.8	99.7
		DSR	95.4	96.2	96.9	97.7	98.5	97.7	99.2	99.2	98.8	98.5

application perspective, this is a "second-order effect" because, in both cases, the BERs are quite low and the SSRs are high.

4.2.2 *BC-IBs*

For BC-IBs, we use all the 18 keyframes with varied backgrounds for our experiments. As in the case of RGB-CWBs, we captured two separate sets of QR code embedded BC-IBs for all combinations of displays, smartphones, and barcode modes. The resulting dataset consists of 2304 BC-IBs and 2304 baseline BW-Bs.

Table 5 shows the average BER, DSR, and SSR for QR code embedded BC-IBs and baseline BW-Bs. The BC-IBs have lower BER in comparison with baseline BW-Bs for both couch potato and active viewer modes. The SSR and DSR for BC-IBs are marginally less than baseline BW-Bs. For the active viewer mode, the DSR for BC-IBs is marginally better than baseline BW-Bs.

Table 5 Average percent BER, SSR, and DSR for QR BC-IBs and baseline QR BW-Bs.

Barcode mode	Method	BER (%)	SSR (%)	DSR (%)
Couch potato	Image barcode	0.72	99.1	99.5
	Baseline	0.92	99.7	99.6
Active viewer	Image barcode	0.59	99.5	98.7
	Baseline	0.85	99.7	98.5

4.2.3 *Barcode performance in the presence of compression*

The performance of the proposed approaches was additionally evaluated in the presence of typical compression. The experiments were conducted on four displays (L3, D1, T1, and V1) and three smartphones (M1, S1, and A1). For a selected combinations of displays and smartphones, data recovery performance under JPEG compression (at a quality factor of 75) is evaluated for coherent/incoherent RGB-CWBs and BC-IBs and compared with baseline BW-Bs.

Table 6 Performance of the proposed RGB-CWBs and comparison against the baseline in the presence of JPEG compression (at a quality factor of 75). For a description of the reported metrics and schemes, see the caption for Table 3.

			Estimated red			Estimated green			Estimated blue			
			IC			IC			IC			
Barcode mode	Error corr. level	Metrics (%)	Linear	Affine	No IC	Linear	Affine	No IC	Linear	Affine	No IC	Baseline
Couch potato	L	BER	0.05	0.05	0.99	1.52	0.03	0.26	0.05	0.04	0.47	0.004
		BER*	0.04	0.05	0.99	1.56	0.03	0.20	0.04	0.03	0.47	—
		SSR	100	100	86.9	82.6	82.6	91.3	100	100	89.1	100
		DSR	100	100	90.0	86.8	92.1	92.9	100	100	95.1	100
	Q	BER	0.31	0.32	1.49	0.02	0.03	0.58	0.38	0.34	1.08	0.93
		BER*	0.20	0.26	1.49	0.02	0.02	0.58	0.27	0.24	1.11	—
		SSR	91.7	91.7	70.8	100	100	97.9	97.9	97.9	83.3	100
		DSR	100	100	85.3	100	100	100	100	100	97.5	100
Active viewer	L	BER	0.23	0.20	0.50	0.03	0.03	0.08	0.22	0.23	1.18	0.08
		BER*	0.23	0.20	0.50	0.03	0.03	0.08	0.22	0.23	1.20	—
		SSR	100	100	100	94.3	94.3	90	100	98.6	100	100
		DSR	98.6	98.6	91.4	95.5	92.4	82.5	98.6	97.1	81.42	100
	Q	BER	0.73	0.69	1.32	0.05	0.06	0.14	0.45	0.45	1.17	1.22
		BER*	0.57	0.53	1.34	0.05	0.06	0.14	0.37	0.37	1.17	—
		SSR	97.2	100	94.4	100	100	100	100	100	88.9	100
		DSR	94.3	97.2	88.2	100	100	91.7	100	100	100	98.9

Table 6 shows the average percentage BER, BER*, SSR, and DSR under compression for red, green, and blue channel estimates of QR coherent and incoherent RGB-CWBs and baseline BW-Bs for different modes and error correction levels. We can observe that the impact of compression on the red, green, and blue channel estimates of coherent/incoherent RGB-CWBs is minimal when compared with corresponding data recovery performance of RGB-CWBs under no compression (presented in Tables 3 and 4).

Table 7 Average percent BER, SSR, and DSR under compression for QR BC-IBs and baseline QR BW-Bs.

Barcode mode	Method	BER (%)	SSR (%)	DSR (%)
Couch potato	Image barcode	1.09	99.3	97.9
	Baseline	1.23	100	100
Active viewer	Image barcode	1.05	98.6	97.1
	Baseline	0.84	100	100

Table 7 shows the average BER, DSR, and SSR under compression for QR code embedded BC-IBs and baseline BW-Bs. We can observe that BC-IBs under compression have slightly higher BER and, similar SSR and DSR when compared with data recovery metrics for the BC-IBs under no compression.

5 Conclusion

We proposed a CW barcode framework for color display applications and focused on two advantageous realizations of the framework: RGB-CWBs and BC-IBs. RGB-CWBs provide a three-fold increase in data capacity, whereas BC-IBs significantly reduce the perceptual impact, when compared with BW-Bs. Based on exhaustive experimentation across multiple displays and smartphones, we analytically demonstrated the advantages of CW barcodes. Visual distortion is ~50% lower for BC-IBs and marginally worse for RGB-CWBs when compared with BW-Bs. For QR RGB-CWBs, the BER is under 3.14% even without IC and further reduced by the proposed IC techniques. The synchronization and DSR for CW barcodes is comparable with BW-Bs. CW barcodes offer a general framework that can be used with any pre-existing BW-B design and with any selections of the display and capture image channels. The BC-IB realizations within this framework offer a particularly attractive alternative for significantly reducing the perceptual obtrusiveness of in-video embedded barcodes.

6 Discussion

The versatility of the CW display barcode framework proposed in this paper has already been partly highlighted in the preceding sections. Specifically, the framework enables an existing BW-B to be advantageously converted into either of the RGB-CWB or BC-IB realizations through reuse of existing design elements for localization, synchronization, data encoding, and error correction. Although we focus on these two realizations because they have the most potential, additional alternatives can also be realized in the CW framework. Clearly alternatives that use two channels or a single channel other than the blue channel are also feasible within the proposed framework. Specifically, analogous to BC-IB, green and red-channel IBs can also be realized and dynamically selecting between these options, based on image content, can offer opportunities for reducing visual distortion.[36] Note that while BC-IBs significantly reduce distortion in comparison with BW-Bs, the presence of the embedded barcode is clearly apparent in the image (see Fig. 8). This is actually helpful because, in the absence of a visual indicator, users may not realize that they can interact with the displayed image using a mobile device, a problem often faced by invisible watermarks.[1] A potential challenge with BC-IBs is that users may not immediately recognize that a barcode is embedded. To address this issue an initial phase of "user education" may be necessary to make them aware that they can use the barcode much like they use the monochrome versions. Additionally, to get users acclimatized, in an initial transition period, the BC-IBs may be used with the localization pattern retained in all channels to allow users to readily recognize that a barcode is present.

Compared to coherent RGB-CWBs, incoherent RGB-CWBs offer design flexibility that can be advantageously exploited. Because the incoherent designs do not require the barcodes embedded in the three channels to share a common geometry, the individual barcodes can be independently designed without requiring coordination. In display advertising, as the primary image/video content is transmitted from its originating source to the final display, individual channel barcodes can be inserted at different points in space and time to produce an incoherent RGB-CWB. For instance, when a traditional commercial broadcasting network distributes content through several local affiliate television stations, the incoherent design allows the network and the local affiliate to independently insert their advertisement barcodes in distinct channels. Aside from display advertising, the flexibility can also be advantageously used to multiplex two or

Table 8 Mean and saliency-weighted-mean S-CIELAB-CIEDE2000 ΔE estimates for the proposed Aztec code embedded CW barcodes and baseline Aztec BW-Bs. For a description of reported metrics and schemes, see the caption for Table 2.

			Mean ΔE				Salience weighted mean ΔE			
Barcode mode	Display size/resolution (in./ppi)	Viewing distance (in.)	BC-IB	Coherent RGB-CWB	Incoherent RGB-CWB	Baseline BW-B	BC-IB	Coherent RGB-CWB	Incoherent RGB-CWB	Baseline BW-B
Couch potato	15/105 (L1)	21	1.10	2.23	2.25	2.20	0.35	0.71	0.71	0.69
	13.5/227 (L2)	19	1.19	2.29	2.31	2.24	0.39	0.73	0.74	0.71
	13.3/267 (L3)	19	1.22	2.32	2.34	2.25	0.40	0.74	0.75	0.72
	9.7/264 (T1)	15	1.17	2.28	2.30	2.23	0.38	0.73	0.73	0.71
	20/82 (C1), 18/91 (D2)	30, 27	1.11	2.24	2.26	2.21	0.36	0.71	0.71	0.70
	106/21 (P1), 60/37 (V1), 24/92 (D1)	159, 90, 36	1.14	2.25	2.28	2.21	0.37	0.71	0.72	0.70
Active viewer	15/105 (L1)	21	0.45	0.79	0.77	0.75	0.40	0.72	0.71	0.68
	13.5/227 (L2)	19	0.53	0.85	0.84	0.80	0.48	0.78	0.76	0.73
	13.3/267 (L3)	19	0.56	0.88	0.86	0.83	0.50	0.80	0.78	0.75
	9.7/264 (T1)	15	0.51	0.84	0.83	0.79	0.46	0.76	0.75	0.72
	20/82 (C1), 18/91 (D2)	30, 27	0.45	0.79	0.78	0.75	0.41	0.72	0.71	0.68
	106/21 (P1), 60/37 (V1), 24/92 (D1)	159, 90, 36	0.48	0.81	0.80	0.77	0.44	0.74	0.73	0.69

more independent barcodes in the same spatial footprint. This functionality can support alternative payment systems for point of sale (such as WeChat Pay and AliPay[52] that are commonly used alternatives in China) and different languages.

7 Appendix

In this section, we provide experimental results for tests conducted with Aztec barcodes, i.e., for RGB-CWB and BC-IB constructions built using the monochrome Aztec code, which is also used as the baseline for comparison. These results complement the results presented for the QR codes in the main paper and demonstrate another powerful advantage of the CW framework; the framework can flexibly be used in conjunction with any BW-B design. Additionally, we also summarize the variability in cross-channel interference observed in our experiments.

7.1 *Visual Distortion for Aztec Barcodes*

Similar to QR CW barcodes, a total of 144 Aztec CW barcodes were used for visual distortion experiments. As shown in Table 8, the visual distortion result for the Aztec CW barcodes is similar to QR CW barcodes, with average ΔE and saliency weighted ΔE values for BC-IBs significantly lower than for the baseline BW-Bs.

7.2 *Data Recovery Performance for Aztec Barcodes*

7.2.1 *RGB-CWB*

We note that the QR codes have a robust design layout with multiple synchronization patterns spread out over the barcode footprint, which enables accurate correction of perspective distortion, providing greater flexibility in capture orientation compared with the Aztec code where the synchronization pattern is more localized and less effective for estimating perspective distortion. In mobile phone apps for reading Aztec codes, this shortcoming can be overcome by requiring the user to better orient the capture camera. To improve synchronization performance in our experiments with Aztec CW barcodes, after IC, we perform an additional reconstruction process before decoding the data. For reconstruction, we first binarize the interference canceled individual channel estimates. We calculate the module size of the binarized barcode and then perform module-by-module reconstruction to obtain reconstructed barcode,

Table 9 Performance of the proposed Aztec coherent RGB-CWBs decoded using PB IC and without any IC, and comparison against the baseline BW-Bs. For a description of the reported metrics and schemes, see the caption for Table 3.

			Estimated red			Estimated green			Estimated blue			
			IC			IC			IC			
Barcode mode	Error corr. level	Metrics (%)	PB linear	PB affine	No IC	PB linear	PB affine	No IC	PB linear	PB affine	No IC	Baseline
Couch potato	L	BER	0.52	0.52	0.78	0.37	0.36	0.60	0.70	0.71	0.93	0.34
		BER*	0.52	0.52	0.78	0.37	0.36	0.60	0.70	0.70	0.89	—
		SSR	100	100	100	99.0	99.0	99.0	98.1	99.0	99.0	99.7
		DSR	100	100	99.0	100	100	100	98.0	98.1	97.1	100
	Q	BER	2.12	2.10	1.71	1.35	1.36	1.57	2.04	2.09	2.11	0.42
		BER*	2.14	2.12	1.71	1.35	1.36	1.57	2.00	2.00	1.90	—
		SSR	100	100	99.0	98.1	98.1	98.1	97.1	100	98.1	99.7
		DSR	98.1	98.1	100	100	100	100	97.0	96.2	95.1	100
Active viewer	L	BER	1.98	1.98	2.20	0.54	0.55	0.72	0.64	0.63	0.99	1.75
		BER*	1.98	1.98	2.20	0.54	0.54	0.72	0.64	0.63	0.99	—
		SSR	100	100	100	99.2	99.2	97.5	97.5	97.5	96.7	99.2
		DSR	95.8	95.8	93.3	99.2	99.2	99.2	100	100	95.7	100
	Q	BER	3.56	3.57	3.99	2.16	2.23	2.31	2.68	2.64	3.12	2.27
		BER*	3.56	3.57	4.01	2.20	2.10	2.31	2.68	2.64	2.95	—
		SSR	98.3	98.3	99.2	96.7	97.5	95	97.5	97.5	99.2	98.4
		DSR	94.9	94.9	88.2	94.8	97.4	96.5	97.4	97.4	95.0	100

Table 10 Performance of the proposed Aztec incoherent RGB-CWBs decoded using EM IC and without any IC, and comparison against the baseline BW-Bs. For a description of the reported metrics and schemes, see the caption for Table 3.

Barcode mode	Error corr. level	Metrics (%)	Estimated red			Estimated green			Estimated blue			Baseline
			IC			IC			IC			
			EM linear	EM affine	No IC	EM linear	EM affine	No IC	EM linear	EM affine	No IC	
Couch potato	L	BER	0.63	1.08	1.25	0.55	0.70	0.21	0.25	0.23	0.69	0.34
		BER*	0.63	1.08	1.25	0.55	0.70	0.21	0.26	0.24	0.69	—
		SSR	100	100	100	100	100	100	98.1	99.0	96.1	99.7
		DSR	97.1	97.1	93.2	100	100	100	100	100	100	100
	Q	BER	1.83	1.68	2.14	2.29	2.15	2.17	0.68	0.61	0.95	0.42
		BER*	1.83	1.68	2.14	2.29	2.15	2.17	0.72	0.67	0.94	—
		SSR	100	100	100	100	100	100	99.0	99.0	90.4	99.7
		DSR	100	100	96.2	100	100	100	100	100	98.9	100
Active viewer	L	BER	0.31	0.31	2.19	1.00	1.08	0.84	0.41	0.38	0.72	1.75
		BER*	0.31	0.31	2.19	0.97	1.05	0.84	0.41	0.38	0.71	—
		SSR	100	100	100	100	100	99.2	99.2	99.2	100	99.2
		DSR	99.2	99.2	93.3	97.5	98.3	98.3	100	100	98.3	100
	Q	BER	1.21	1.11	1.29	2.06	2.07	2.57	0.56	0.60	0.44	2.27
		BER*	1.21	1.11	1.29	2.06	2.07	2.57	0.58	0.54	0.44	—
		SSR	100	100	100	100	100	100	100	100	96.7	98.4
		DSR	98.3	98.3	96.6	98.3	98.3	97.5	100	100	100	100

which is fed to the decoder. This reconstruction process significantly improves the ability to synchronize.

The data recovery experiments for the Aztec codes had 1120 captured images of RGB-CWBs and 1536 captured images of baseline BW-Bs, over the same display smartphone combinations as were used for the QR codes (listed in Table 1). Tables 9 and 10 show the average BER, BER*, SSR, and DSR for the red, green, and blue channels for the CW Aztec coherent and incoherent RGB-CWBs, respectively. The structure of these tables is identical to that used for the QR codes and described earlier. The tabulated statistics for the Aztec RGB-CWBs show trends similar to those observed for the QR RGB-CWBs. The data recovery performance of the Aztec RGB-CWBs is only slightly worse than the baseline BW-Bs. Using the PB/EM IC techniques is advantageous resulting in a lower BER and improved SSR/DSR in comparison with the same metrics when decoded without IC.

7.2.2 *BC-IB*

The data recovery experiments for the Aztec codes had 1152 captured images of BC-IBs and 1152 captured images of baseline BW-Bs, over the same display smartphone combinations as were used for the QR codes (listed in Table 1). Table 11 shows the average BER, DSR, and SSR for Aztec BC-IBs and baseline BW-Bs. For the couch potato mode, the BER for BC-IBs is higher than for the baseline BW-Bs, whereas for the active viewer mode the BC-IBs perform better with lower BER than baseline BW-Bs. The SSR and DSR for BC-IBs are comparable with the SSR and DSR for baseline BW-Bs. For the active viewer mode, we can observe that SSR for BC-IBs is marginally better than baseline BW-Bs.

Table 11 Average percent BER, SSR, and DSR for Aztec BC-IBs and baseline BW-Bs.

Barcode mode	Method	BER (%)	SSR (%)	DSR (%)
Couch potato	Image barcode	0.54	100	100
	Baseline	0.31	100	100
Active viewer	Image barcode	1.55	99.6	100
	Baseline	1.92	99.4	100

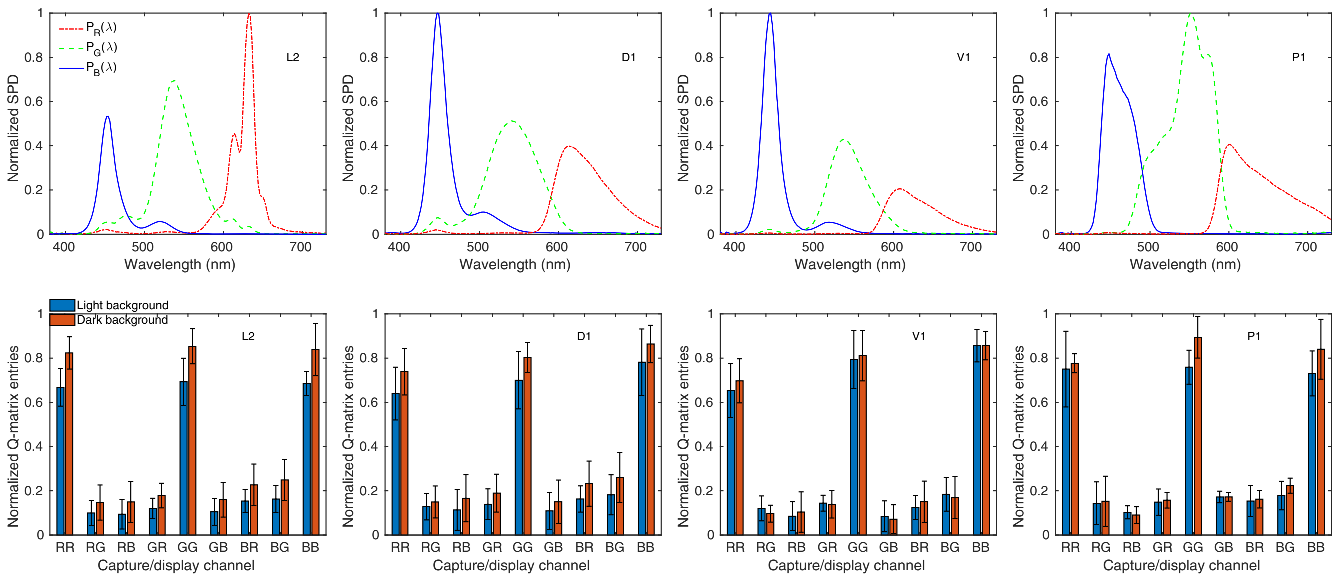

Fig. 10 Normalized spectral power distributions for the R, G, B primaries for four of the displays, viz. laptop (L2), desktop (D1), television (V1), and projector (P1) (top row), and corresponding averaged entries (max normalized to 1) for the cross-channel interference matrix ($\hat{\mathbf{Q}}$) for images corresponding to light and dark backgrounds (bottom row).

7.2.3 *Variation in the cross-channel interference matrix* $\mathbf{Q}$

Our experiments revealed that the cross-channel interference depended both on the specific display-smartphone combination used, and on the image background. To illustrate this effect, we consider the embedded QR codes in two of the test images, in which the image background region adjacent to the barcode was lighter in one image and darker in the other. Averages of the estimated cross-channel interference matrices $\hat{\mathbf{Q}}$ from captured images of these displayed RGB-CWBs are depicted in Fig. 10, where the averages (over different barcode modes, error correction levels, and capture smartphones) of the nine individual entries in $\hat{\mathbf{Q}}$ are shown as bar plots with standard deviation error bars. The relative spectral power distributions for the R, G, and B primaries for the four displays, viz., laptop (L2), desktop (D1), television (V1), and projector (P1) are also included within this figure (measured using a spectroradiometer). The captured images with the dark background exhibit higher values for the cross-channel terms (RG, RB, BR, BG, GR, and GB, where the first letter denotes the capture channel and the second letter denotes the display channel), indicating higher cross-channel interference in the presence of dark backgrounds (Although the corresponding channel RR, GG, and BB values are also higher, the relative magnitudes of the cross-channel interference is higher.). Also the variation in the characteristics of different displays results in significant variation in the entries of the cross-channel interference matrix, highlighting the need for and benefit of the proposed methods for estimating the cross-channel interference on-the-fly, directly from the captured barcode image.

Acknowledgments

This work was supported in part by a distinguished researcher award from the New York state funded Rochester Center of Excellence in Data Science (Contract CoE #3B C160189) at the University of Rochester. Shingirai Dhoro's work on this research was supported in part by a Xerox Engineering Research Fellowship at the University of Rochester. We thank the associate editor and the anonymous reviewers, their comments and suggestions have helped to significantly improve this paper.

References

1. G. Sharma, "Image-based data interfaces revisited: Barcodes and watermarks for the mobile and digital worlds," in *8th Intl. Conf. Comm. Sys. and Networks (COMSNETS)*, Bangalore, India, pp. 1–6 (2016).
2. N. Damera-Venkata et al., "Hardcopy image barcodes via block-error diffusion," *IEEE Trans. Image Proc.* **14**, 1977–1989 (2005).
3. O. Bulan, G. Sharma, and B. Oztan, "High capacity image barcodes using color separability," *Proc. SPIE* **7866**, 78660N (2011).
4. ISO/IEC, "Information technology—automatic identification and data capture techniques—QR code 2005 bar code symbology specification," 2006, http://www.iso.org/iso/iso_catalogue/catalogue_ics/catalogue_detail_ics.htm?csnumber=43655 (accessed Jan 2011).
5. ISO/IEC, "Information technology—automatic identification and data capture techniques—Aztec code bar code symbology specification," 2008, http://www.iso.org/iso/iso_catalogue/catalogue_tc/catalogue_detail.htm?csnumber=41548 (accessed April 2011).
6. A. Longacre and R. Hussey, "Two dimensional data encoding structure and symbology for use with optical readers," US Patent 5, 591, 956 (1997).
7. M. Rohs, "Real-world interaction with camera phones," in *Int. Symp. Ubiquitious Comput. Syst.*, Springer, pp. 74–89 (2004).
8. D. Scott et al., "Using visual tags to bypass bluetooth device discovery," *SIGMOBILE Mob. Comput. Commun. Rev.* **9**, 41–53 (2005).
9. M. Fetter, C. Beckmann, and T. Gross, "Magneticode: physical mobile interaction through time-encoded magnetic identification tags," in *Proc. 8th Int. Conf. Tangible, Embedded and Embodied Interact., TEI '14*, ACM, New York, NY, USA, pp. 205–212 (2013).
10. D. E. Wood, "Methods for encoding and decoding information," US Patent 7, 516, 904 (2009).
11. B. Zhang et al., "SBVLC: secure barcode-based visible light communication for smartphones," in *IEEE INFOCOM Proc.*, pp. 2661–2669 (2014).
12. F. Hermans et al., "Focus: robust visual codes for everyone," in *Proc. 14th Ann. Int. Conf. Mob. Syst. Appl. and Serv.*, ACM, pp. 319–332 (2016).
13. W. Hu et al., "Strata: layered coding for scalable visual communication," in *Proc. 20th Ann. Int. Conf. Mob. Comput. and Networking*, ACM, pp. 79–90 (2014).
14. N. Halpin, "Walmart launches mobile payments processor," *Business Insider*, 14 December 2015, http://www.businessinsider.com/walmart-launches-mobile-payments-processor-2015-12?IR=T.

15. S. Ramakrishnan and N. Bose, "Walmart adds to mobile wallet frenzy with walmart pay," Reuters, 10 December 2015, http://www.reuters.com/article/us-wal-mart-mobilepayment-idUSKBN0TT0E620151210.
16. D. Parikh and G. Jancke, "Localization and segmentation of a 2-D high capacity color barcode," in *IEEE Workshop Appl. of Comput. Vision, WACV 2008.*, IEEE, pp. 1–6 (2008).
17. O. Bulan, H. Blasinski, and G. Sharma, "Color QR codes: increased capacity via per-channel data encoding and interference cancellation," in *Proc. IS&T/SID Nineteenth Color and Imaging Conf.: Color Sci. and Eng. Syst., Technol. and Appl.*, San Jose, CA, pp. 156–159 (2011).
18. R. John and K. Raahemifar, "Designing a 2D color barcode," in *28th IEEE Canadian Conf. Electr. and Comput. Eng.*, pp. 297–301 (2015).
19. H. Blasinski, O. Bulan, and G. Sharma, "Per-colorant-channel color barcodes for mobile applications: an interference cancellation framework," *IEEE Trans. Image Proc.* **22**, 1498–1511 (2013).
20. T. Hao, R. Zhou, and G. Xing, "COBRA: color barcode streaming for smartphone systems," in *Proc. 10th Int. Conf. Mob. Syst. Appl. and Serv.*, ACM, pp. 85–98 (2012).
21. T. Langlotz and O. Bimber, "Unsynchronized 4d barcodes," in *Int. Symp. Vis. Comput.*, Springer, pp. 363–374 (2007).
22. Q. Wang et al., "Rain bar: robust application-driven visual communication using color barcodes," in *35th Int. Conf. Distrib. Comput. Syst. (ICDCS)*, IEEE, pp. 537–546 (2015).
23. X. Liu, D. Doermann, and H. Li, "VCode-pervasive data transfer using video barcode," *IEEE Trans. Multimedia* **10**, 361–371 (2008).
24. W. Huang and W. H. Mow, "PiCode: 2D barcode with embedded picture and ViCode: 3D barcode with embedded video," in *Proc. 19th Ann. Int. Conf. Mob. Comput. Networking*, ACM, pp. 139–142 (2013).
25. C. Chen et al., "PiCode: a new picture-embedding 2D barcode," *IEEE Trans. Image Proc.* **25**, 3444–3458 (2016).
26. H. Tack-Don et al., "Machine readable code image and method of encoding and decoding the same," US Patent 7, 020, 327 (2006).
27. C. Cheong et al., "Pictorial image code: a color vision-based automatic identification interface for mobile computing environments," in *Eighth IEEE Workshop Mob. Comput. Syst. and Appl., HotMobile*, pp. 23–28 (2007).
28. Y.-H. Lin, Y.-P. Chang, and J.-L. Wu, "Appearance-based QR code beautifier," *IEEE Trans. Multimedia* **15**(8), 2198–2207 (2013).
29. Z. Baharav and R. Kakarala, "Visually significant QR codes: image blending and statistical analysis," in *IEEE Int. Conf. Multimedia and Expo (ICME)*, IEEE, pp. 1–6 (2013).
30. G. J. Garateguy et al., "QR images: optimized image embedding in QR codes," *IEEE Trans. Image Proc.* **23**(7), 2842–2853 (2014).
31. E. Olson, "Bar codes add detail on items in TV ads," *The New York Times*, 27 September 2010, http://www.nytimes.com/2010/09/27/business/media/27bluefly.html?module=ArrowsNav&contentCollection=Media&action=keypress&region=FixedLeft&pgtype=article.
32. "TV shopping barcode advertising banners," http://scan2buy.co.uk/tv_shopping_barcode_advertising_banners/tv_shopping_barcode_advertising_banners.
33. N. Arce, "Motorola updates camera and gallery apps, now allows QR code scanning and saving albums to MicroSD," *Tech Times*, 31 August 2015, http://www.techtimes.com/articles/80661/20150831.
34. F. Tepper, "The iPhone's camera app can now read QR codes," *Tech Crunch*, 5 June 2017, https://techcrunch.com/2017/06/05/the-iphones-camera-app-can-now-read-qr-codes/.
35. R. Holmes, "Why the" hidden" update in Apple's latest iOS changes the rules of marketing," *Forbes*, 30 October 2017, https://www.forbes.com/sites/ryanholmes/2017/10/30/why-the-hidden-update-in-apples-latest-ios-changes-the-rules-of-marketing.
36. K. Dinesh and G. Sharma, "Display image-barcodes using blue/red channel embedding," in *Electron. Imaging: Media Watermarking, Secur. and Forensics*, IS&T, pp. 159–1–159–7(7) (2018).
37. K. Dinesh and G. Sharma, "Per-channel color barcodes for displays," in *IEEE Int. Conf. Image Proc. (ICIP)*, pp. 3992–3996, IEEE (2016).
38. N. Murphy, "Op-ed: why the barcode will soon become the world's largest consumer engagement platform," https://www.psfk.com/2018/03/niall-murphy-evrythng-barcode.html.
39. S. Wang, "Why China can't get enough of QR codes," https://money.cnn.com/2017/09/08/technology/china-qr-codes/index.html.
40. K. Chiu, "How the QR code conquered China." https://www.abacusnews.com/who-what/how-qr-code-conquered-china/article/2136537.
41. J. G. Proakis and M. Salehi, *Digital Communications*, vol. **4**, McGraw-hill, New York (2001).
42. C. M. Bishop, *Pattern Recognition and Machine Learning*, Springer (2006).
43. N. Otsu, "A threshold selection method from gray-level histograms," *IEEE Trans. Syst. Man Cybern.* **9**(1), 62–66 (1979).
44. J. Le Feuvre et al., "Ultra high definition HEVC DASH data set," in *Proc. 5th ACM Multimedia Syst. Conf.*, pp. 7–12 (2014).
45. S. Lin and D. J. Costello Jr., *Error Control Coding*, Prentice-Hall, Englewood Cliffs, New Jersey (2004).
46. X. Zhang and B. A. Wandell, "A spatial extension of CIELAB for digital color-image reproduction," *J. Soc. Inf. Disp.* **5**(1), 61–63 (1997).
47. M. R. Luo, G. Cui, and B. Rigg, "The development of the CIE 2000 colour-difference formula: CIEDE2000," *Color Res. Appl.* **26**, 340–350 (2001).
48. G. Sharma, W. Wu, and E. N. Dalal, "The CIEDE2000 color-difference formula: implementation notes, supplementary test data, and mathematical observations," *Color Res. Appl.* **30**, 21–30 (2005).
49. CIE, "Colorimetry," CIE Publication No. 15.2, Central Bureau of the CIE, Vienna (1986).
50. G. Sharma and C. E. Rodríguez-Pardo, "The dark side of CIELAB," *Proc. SPIE* **8292**, 82920D (2012).
51. B. Schauerte and R. Stiefelhagen, "Quaternion-based spectral saliency detection for eye fixation prediction," in *ECCV 2012*, Springer, pp. 116–129 (2012).
52. I. Fraser, "Chinese payment giants are lightyears ahead," https://www.raconteur.net/finance/alipay-wechat-china-payments.

Karthik Dinesh received his BE degree in electronics and communication from the National Institute of Engineering, Mysore, India, and his MTech degree from the Indian Institute of Technology, Kanpur, India. He is currently pursuing his PhD in the ECE Department at the University of Rochester under the supervision of Dr. Gaurav Sharma.

Jiangfeng Lu is currently pursuing his BS degree in ECE from the University of Rochester. He is interested in digital image processing and embedded systems.

Shingirai Dhoro is an international baccalaureate bilingual diploma graduate from Waterford United World College, Swaziland. He is a current electrical and computer engineering undergraduate at the University of Rochester. His current interests are in the areas of communication systems and signal processing.

Gaurav Sharma is a professor in the Department of Electrical and Computer Engineering, Department of Computer Science, and Department of Biostatistics and Computational Biology at the University of Rochester. He is the editor of the *Digital Color Imaging Handbook*, published by CRC Press in 2003. He is a fellow of the Society of Imaging Science and Technology (IS&T), SPIE, and IEEE, and a member of Sigma Xi.